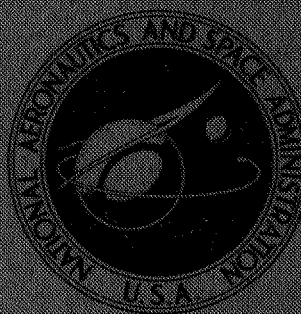


NASA TECHNICAL
MEMORANDUM



NASA TM X-1880

NASA TM X-1880

CASE FILE
COPY

MULTISTAGE COMPRESSOR SIMULATION
APPLIED TO THE PREDICTION
OF AXIAL FLOW INSTABILITIES

by Ross G. Willob and Kurt Seldner

Lewis Research Center

Cleveland, Ohio

1. Report No. NASA TM X-1880	2. Government Accession No.	3. Recipient's Catalog No.	
4. Title and Subtitle MULTISTAGE COMPRESSOR SIMULATION APPLIED TO THE PREDICTION OF AXIAL FLOW INSTABILITIES		5. Report Date September 1969	6. Performing Organization Code
		8. Performing Organization Report No. E-5150	
7. Author(s) Ross G. Willoh and Kurt Seldner		10. Work Unit No. 720-07	11. Contract or Grant No.
9. Performing Organization Name and Address Lewis Research Center National Aeronautics and Space Administration Cleveland, Ohio 44135		13. Type of Report and Period Covered Technical Memorandum	
		14. Sponsoring Agency Code	
12. Sponsoring Agency Name and Address National Aeronautics and Space Administration Washington, D.C. 20546			
15. Supplementary Notes			
16. Abstract A simulation model for the one-dimensional steady state and dynamic performance of an axial flow compressor is presented. The modeling technique is applied to the eight-stage J 85-13 compressor. It is shown that the simulation stability boundary coincides with the compressor stall line. Analytical and experimental results are presented and compared.			
17. Key Words (Suggested by Author(s)) Compressor performance		18. Distribution Statement Unclassified - unlimited	
19. Security Classif. (of this report) Unclassified	20. Security Classif. (of this page) Unclassified	21. No. of Pages 26	22. Price* \$3.00

*For sale by the Clearinghouse for Federal Scientific and Technical Information
Springfield, Virginia 22151

MULTISTAGE COMPRESSOR SIMULATION APPLIED TO THE PREDICTION OF AXIAL FLOW INSTABILITIES

by Ross G. Willoh and Kurt Seldner

Lewis Research Center

SUMMARY

A simulation model for the one-dimensional steady state and dynamic performance of an axial flow compressor is presented. The modeling technique is applied to the eight stage J 85-13 compressor. It is shown that the simulation stability boundary coincides with the compressor stall line. Analytical and experimental results are presented and compared.

INTRODUCTION

The transient performance of aircraft propulsion systems, using axial compressors, is strongly influenced by the compressor stall characteristic. Compressor stall is accompanied by reduced airflow and engine thrust and increased turbine inlet temperature. In supersonic applications the reduced airflow can result in the inlet unstating. The ability to adequately predict stall and to evaluate the effects of operational parameters on engine stall characteristics is thus of considerable significance in propulsion system design.

As indicated in reference 1, there is a minimum flow point for each compressor operating speed, where the compressor will stall. The locus of minimum flow points defines a compressor stall line. Jet engine fuel controls schedule propulsion system parameters to maintain engine operation along an operating line which is below the stall line. The separation between the stall and steady state operating lines represents engine stall margin.

During acceleration from one steady state condition to another, engine operation follows a path from the steady state operating line toward the stall line and back. If the acceleration time is to be minimized, the stall margin during the transient must be small. Knowledge of the compressor stall line is thus of great importance in the design of pro-

out the text are defined in appendix A.

The analysis assumes that each stage, consisting of a rotor, a stator, and an included volume, can be modeled by a compressor element coupled to the gas dynamics of a lumped volume element. The compressor element is assumed to instantaneously satisfy the stage steady-state characteristics in response to the conditions imposed by the adjacent volumes. The details of the mathematical representation of the steady-state stage performance are presented in appendix B, and the equations for the lumped volume gas dynamics are developed in appendix C.

Steady-State Characteristics

The prediction of the off design steady-state performance of a multistage axial flow compressor is a complex problem. The inclusion of gas dynamics, required to examine system stability, further complicates the problem. Reference 1 includes discussions of the blade element method, stage-stacking techniques, and the use of performance data from existing compressors for the prediction of off design compressor performance. Of the three techniques, only the stage-stacking method combines easily with lumped volume dynamics to form an overall dynamic compressor model. The analysis of compressor dynamics presented in this report is thus based on the stage stacking method for the steady-state portion of the model.

The steady-state performance of the individual stages of a multistage compressor can be represented by pressure and temperature rise coefficients ψ_c^P and ψ_c^T , which are functions of the flow coefficient Φ_c . These coefficients are mathematically defined for the n^{th} stage in appendix B as

$$\psi_{c,n}^P = \frac{C_n T_{tv,n-1}}{N^2} \left[\left(\frac{P_{tc,n}}{P_{tv,n-1}} \right)^{2/7} - 1 \right] \quad (1)$$

$$\psi_{c,n}^T = \frac{C_n}{N^2} (T_{tc,n} - T_{tv,n-1}) \quad (2)$$

$$\Phi_{c,n} = \frac{K_n}{N} v_{zc,n} \quad (3)$$

where

$$C_n = \frac{2gJC_p(\alpha)^2}{\pi^2 r_n^2} \quad (4)$$

$$K_n = \frac{\alpha}{\pi r_n} \quad (5)$$

It is shown in appendix B that the axial velocity v_z can be related to the stage inlet static pressure, static temperature, and flow by

$$v_{zc, n} = \frac{\dot{W}_{c, n} T_{sv, n-1} R}{A_{c, n} P_{sv, n-1}} \quad (6)$$

The coefficients ψ^T and ψ^P of equations (1) and (2), however, are defined in terms of total pressures and temperatures. An equation relating v_z to stage inlet total pressure and temperature is developed in appendix B as

$$\frac{\dot{W}_{c, n} \sqrt{\Theta_{v, n-1}}}{\delta_{v, n-1} A_{c, n}} = \frac{v_{zc, n}}{\sqrt{\Theta_{v, n-1}}} \left[1 - \left(\frac{v_{zc, n}}{\sqrt{\Theta_{v, n-1}}} \right)^2 \frac{1}{2gJC_p T_{tr} \cos^2 \beta_n} \right]^{5/2} \rho_{tr} \quad (7)$$

where δ and Θ are total pressure and temperature ratios defined by

$$\delta_{v, n-1} = \frac{P_{tv, n-1}}{P_{tr}}$$

and

$$\Theta_{v, n-1} = \frac{T_{tv, n-1}}{T_{tr}}$$

The angle β , defined as the angle between the air velocity and the axial direction, is primarily a function of compressor design and speed of rotation.

Dynamic Characteristics

The representation of compressor gas dynamics is based on the assumption that overall compressor dynamics can be simulated by individual lumped volume dynamics for each stage. The individual stage dynamics are assumed to occur in an equivalent stage volume which is located just downstream of the stage's active element. The volume dynamics are modeled with conventional lumped volume techniques.

A schematic drawing of a typical stage with its associated volume is shown in figure 1. Through the application of continuity, momentum, and energy balances to the n^{th} stage, it is shown in appendix C that

$$\frac{d}{dt}(\rho_{sv, n}) = \frac{1}{V_n} (\dot{W}_{c, n} - \dot{W}_{c, n+1}) \quad (8)$$

$$\frac{d}{dt}(\dot{W}_{c, n}) = \frac{A_n g}{L_n} \left(1 + 0.2 M_{v, n}^2\right)^{-7/2} (P_{tc, n} - P_{tv, n}) \quad (9)$$

and

$$\frac{d}{dt}(\rho_{sv, n} T_{tv, n}) = \frac{\gamma}{V_n} (T_{tc, n} \dot{W}_{c, n} - T_{tv, n} \dot{W}_{c, n+1}) \quad (10)$$

The equation of state for the gas in the volume can be written as

$$P_{tv, n} = R \left(1 + 0.2 M_{v, n}^2\right)^{5/2} (\rho_{sv, n} T_{tv, n}) \quad (11)$$

Equations (8) to (11) form a complete set of lumped volume dynamic relations for the n^{th} stage volume.

Computer Solution

Equations (1) to (5) and (7) to (11), when combined with the appropriate stage maps, form a set for the n^{th} compressor stage. This set provides a mathematical representation for both the dynamic and static characteristics of the n^{th} stage of a multistage axial compressor. The computer mechanization of the equations can be accomplished with either analog or digital techniques. The analysis of this report, however, is based pri-

marily on the results of an analog computer simulation. The discussion of the computational techniques will thus be directed primarily toward an analog representation.

The steady-state compressor representation utilizes plots of the normalized pressure coefficient ψ^P and the normalized temperature coefficient ψ^T plotted against the normalized flow coefficient Φ . Figure 2 contains plots of the pressure and temperature coefficients against the flow coefficient for the second stage of the compressor studied. From these curves it can be seen that, for a given stage pressure rise the flow coefficient Φ is, in general, double valued. It is thus necessary to enter the stage maps with the flow function.

Equations (3) and (5) can be used to compute the flow coefficient Φ from the stage inlet weight flow, static pressure and temperature, and the compressor rotational speed. Equation (3) can, however, be rewritten in the form

$$\Phi_{c,n} = K_n \frac{v_{zn} / \sqrt{\Theta_n}}{N / \sqrt{\Theta_n}} \quad (12)$$

The term $v_{z,n} / \sqrt{\Theta_n}$ of equation (12) can then be computed from equation (7). This representation allows the use of total pressure and temperature in computing the flow coef-

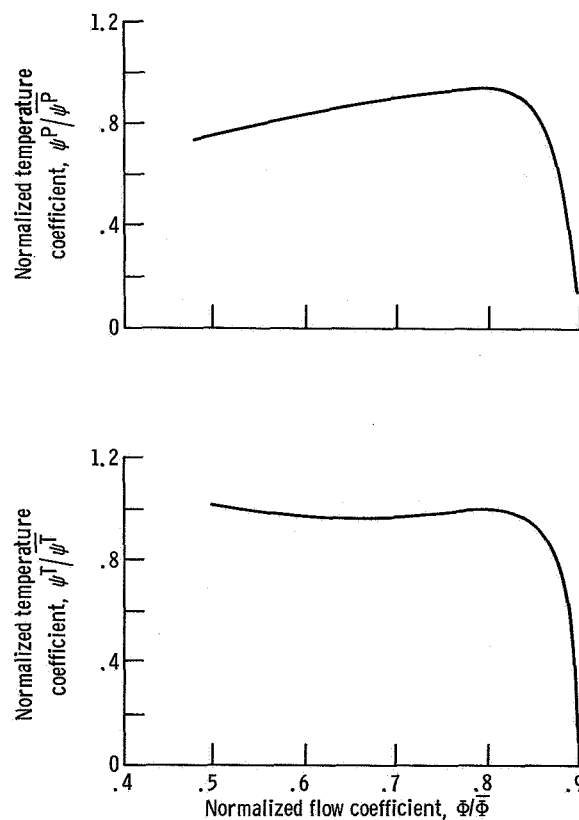


Figure 2. - Pressure and temperature maps for second stage of compressor.

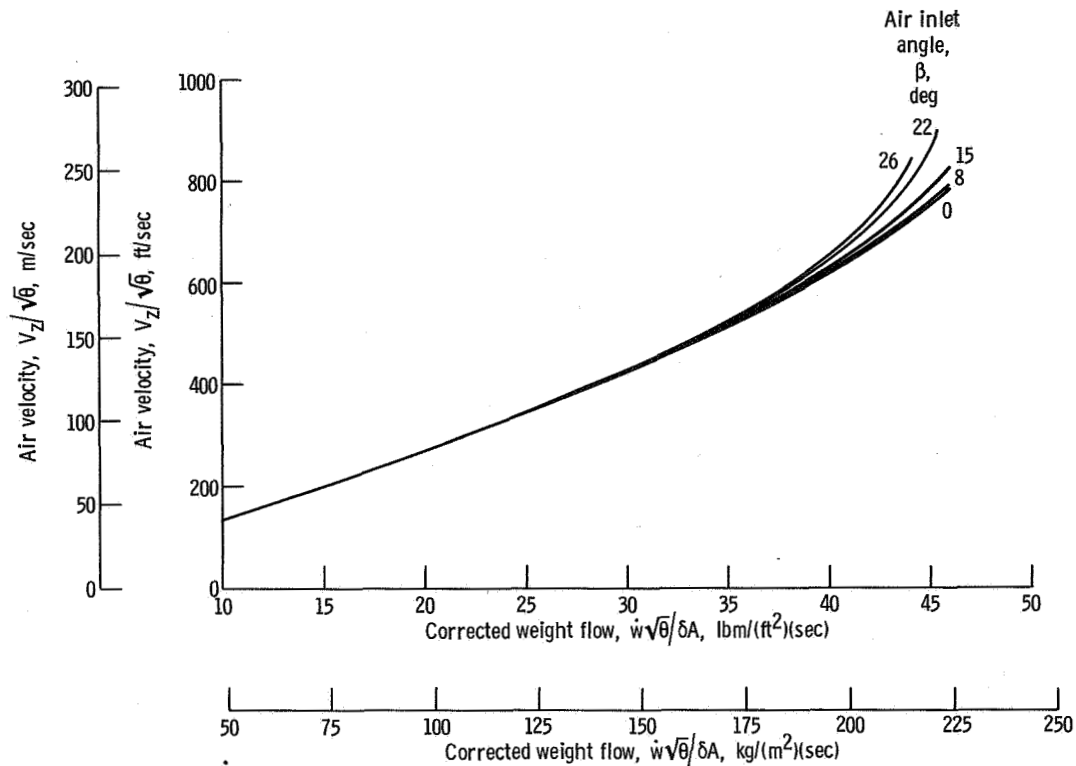


Figure 3. - Air velocity computation.

ficient Φ .

The direct solution of equation (7) for each compressor stage would severely complicate an analog simulation. The axial velocity term $v_z/\sqrt{\Theta}$ computed from equation (7) for various corrected weight flows and rotor air inlet angles is plotted in figure 3. The range of corrected weight flow and rotor air inlet angles included in figure 3 covers the compressor normal operating region. The deviation from a mean value of air inlet angle for stages 2 to 8 of the compressor are plotted as functions of compressor corrected speed $N/\sqrt{\Theta}$ in figure 4. The largest rotor air inlet angle encountered in operation is less than 26° . It can be seen from figure 4 that, with the exception of the second stage, none of the angles vary more than $\pm 2^\circ$ from the mean value as the corrected speed varies from 60 to 100 percent.

It can be seen from figure 3 that the axial velocity to corrected flow characteristic is not extremely sensitive to variations in the air inlet angle. The variation of $\pm 2^\circ$ or less in the air angle for stages 3 to 8 was thus neglected and the stages were assumed to have constant rotor air inlet angles. The second stage air inlet angle varies $9\frac{1}{2}^\circ$ over the 60 to 100 percent speed range. As shown in figure 3, however, the axial velocity to corrected flow characteristic is much less sensitive to changes in the air inlet angle at low mean values of the angle than it is for high mean values. The second stage, which has the lowest mean value of rotor air inlet angle, was also assumed to have a constant rotor air inlet angle.

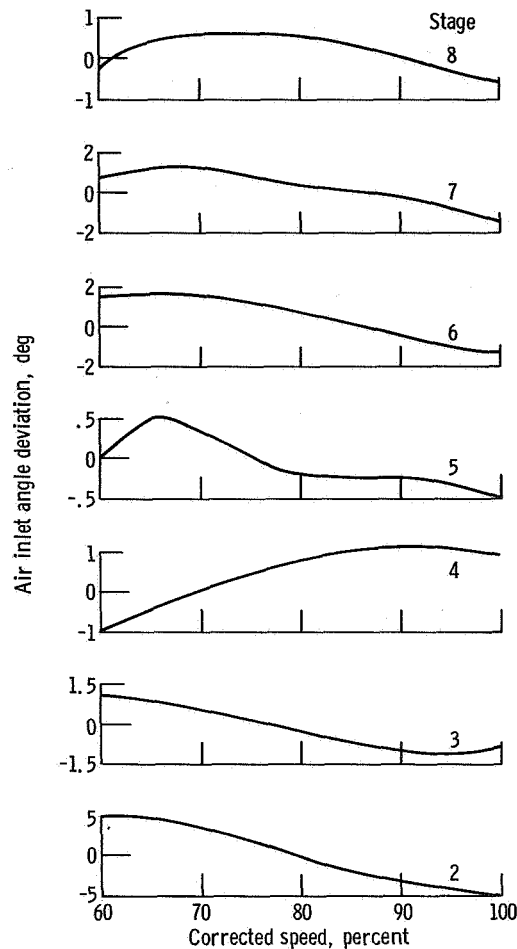


Figure 4. - Deviation of stage rotor air inlet angle from mean.

For the purposes of the computer representation, the axial velocity to weight flow characteristic for each of the stages 2 to 8 was based on a constant mean rotor air inlet angle. The actual simulation used a quadratic curve fitted to the appropriate characteristic.

The J 85-13 compressor contains variable inlet guide vanes ahead of the first compressor stage and variable interstage bleed in the third, fourth, and fifth stage volumes. The two variable geometry features are scheduled, between their extreme limits, as a function of engine corrected speed $N/\sqrt{\theta}$. The variation occurs in the corrected speed range from 80 to 100 percent.

The effects of the variable inlet geometry are included by varying the first stage pressure and temperature coefficients $\psi_{c,1}^P$ and $\psi_{c,1}^T$ as functions of corrected engine speed. Computationally, the variation was achieved by generating the pressure and temperature coefficients as functions of the flow function for the two extremes and an intermediate case and interpolating linearly between the three values for each function.

Although the simulation of the individual stage gas dynamics is essentially based on equations (8) to (11), modifications were included for three of the stages to account for interstage bleed. Further, the distinction between total and static quantities was dropped in the computer representation of the stage dynamics. This simplification, which is discussed in appendix C, is essentially equivalent to eliminating the Mach number terms from equations (9) and (11). With this simplification these equations become

$$\frac{d}{dt}(\dot{W}_{c,n}) = \frac{A_n g}{L_n} (P_{tc,n} - P_{tv,n}) \quad (13)$$

$$P_{tv,n} = R(\rho_{sv,n} T_{tv,n}) \quad (14)$$

The interstage bleed is computed for the third, fourth, and fifth stages by assuming the bleed ports are choked and that the bleed flow can thus be computed from

$$\dot{W}_{b,n} = k_b A_{b,n} \frac{P_{tv,n}}{\sqrt{T_{tv,n}}} \quad (15)$$

The bleed port area $A_{b,n}$ is determined from engine operating schedules. The effects of the bleed flow are included in the stage representation by modifying the continuity balance of equation (8) and the energy balance of equation (10). For the stages with bleed, these equations become

$$\frac{d}{dt}(\rho_{sv,n}) = \frac{1}{V_n} (\dot{W}_{c,n} - \dot{W}_{c,n+1} - \dot{W}_{b,n}) \quad (16)$$

$$\frac{d}{dt}(\rho_{sv,n} T_{tv,n}) = \frac{\gamma}{V_n} (T_{tc,n} \dot{W}_{c,n} - T_{tv,n} \dot{W}_{c,n+1} - T_{tv,n} \dot{W}_{b,n}) \quad (17)$$

A block diagram illustrating the computational sequence used for a typical stage is presented in figure 5. The stage inlet conditions are combined to determine the flow function. The flow function is used to determine the stage pressure and temperature coefficients, and, hence, the stage discharge total pressure and temperature. The discharge conditions are then used with the lumped volume gas dynamics to compute the stage volume gas properties, and, hence, the inlet conditions for the succeeding stage.

The overall J 85-13 compressor representation was formed by interconnecting individual stage representations for each of the eight stages. The first stage maps were

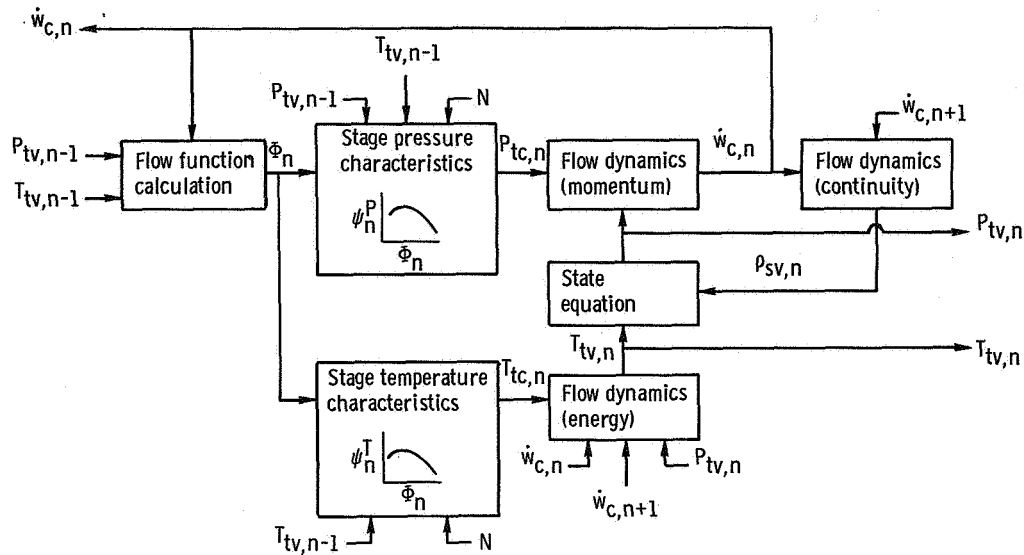


Figure 5. - Block diagram of simulation for n^{th} compressor stage.

modified, as discussed, to account for the variable inlet guide vanes, and bleed flow effects were included in the third, fourth, and fifth stages.

RESULTS AND DISCUSSION

The stage stacking technique used for the representation of the compressor steady-state characteristic requires the simulation of individual stage characteristics for each stage. To simplify the initial simulation, however, it was assumed that the dynamics of several stages could be combined and represented as a single lumped volume element. The stage volumes with interstage bleed ports were individually simulated to maintain the bleed flow dynamics. The dynamics of stages 1 and 2 and the dynamics of stages 6 to 8 were thus combined to form two lumped volume elements.

The compressor simulation was terminated with an equivalent combustor volume and a choked exit station, and the compressor variable geometry was maintained on normal operating schedules. The simulated compressor was then mapped by varying the choked station area at various rotational speeds. With increasing compressor terminating impedance, caused by reductions in the choked station area, the compressor operating point moves along a constant speed line. Figure 6 presents, in schematic form, a typical constant speed operating point locus.

It was found that, as the terminating impedance was increased, the simulation would, at some operating point along the constant speed line, begin to exhibit a limit cycle. Further increases in the impedance resulted in increased limit cycle amplitude. Typical

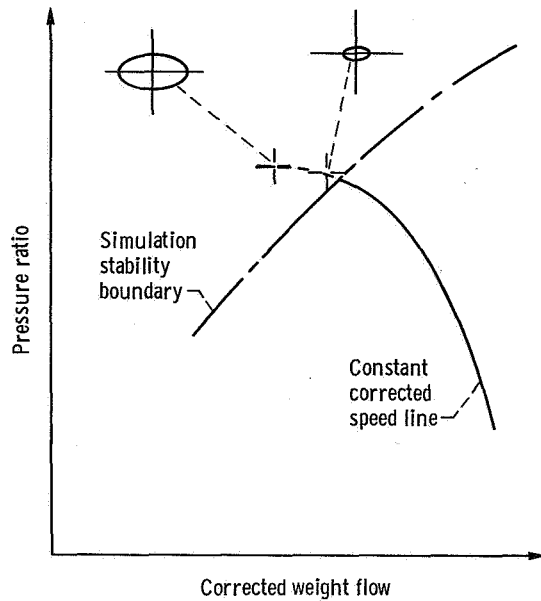


Figure 6. - Schematic of simulation constant speed line and stability boundary.

limit cycle amplitudes are also indicated in figure 6. The limit cycle exhibited hysteresis in that, once the oscillation was established, it was necessary to reduce the terminal impedance beyond the point at which the oscillation first occurred before stable system operation could be reestablished.

A number of constant speed lines were mapped. Noting the operating condition on each speed line where the self-sustained oscillations first occurred allowed the determination of a stability boundary for the compressor simulation. This stability boundary is plotted in figure 7. For reference, the normal stall line for the compressor is included in the figure. The stability boundary resembles, but does not match, the compressor stall line.

Noting that the overall compressor simulation is quite nonlinear, it was concluded that the volume lumping used in the initial simulation was not justified. The simulation was thus revised to include a lumped volume dynamic element for each compressor stage. The stability boundary for the revised simulation was obtained and is also plotted in figure 7. It can be seen that the stability boundary of the compressor simulation falls quite close to the actual compressor stall line when individual stage dynamics are included in the computer representation.

Since the actual compressor stall line, used in the initial portion of the study, was based on minimal data, the technique was applied to operating conditions for which test data was available. Compressor performance and stall line data obtained from tests performed on a J 85-13 engine is presented in reference 5. The experimental results presented in this reference are not representative of standard engine operation. The test re-

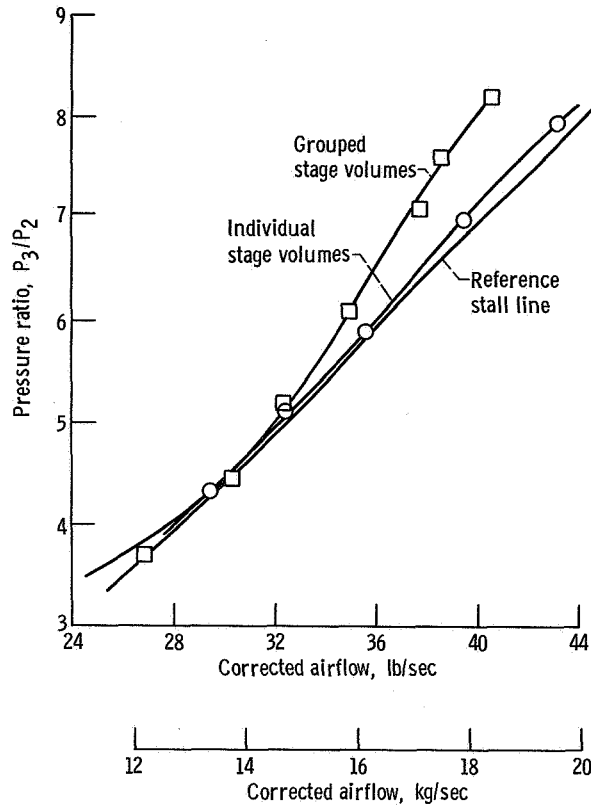


Figure 7. - Compressor stall lines determined from a grouped stage volume simulation and from an individual volume simulation.

sults were obtained with the first stage turbine nozzle area reduced 26 percent, and with the engine variable geometry operated off the normal design schedules.

The tests were performed by maintaining constant engine speed through manual adjustment of the power lever, while the exhaust nozzle area was reduced in small increments. The equilibrium point just prior to compressor stall was defined as the stall point. The procedure was repeated at various engine speeds to obtain the compressor stall line.

The stability boundary for the analog compressor simulation was obtained for the same operating conditions as the test data. The simulated variable geometry was scheduled to match the test conditions, and the terminating impedance was varied while the compressor rotational speed was held constant. Constant speed lines were plotted and the stability boundary was noted. The test data from reference 5 and the results obtained from the simulation with individual stage volume representations are both plotted in figure 8. The good correlation between the experimental and analytical results can be seen in this figure.

Some insight into the overall operation of the compressor in the vicinity of the stability boundary can be gained from examining the normal compressor operating point and

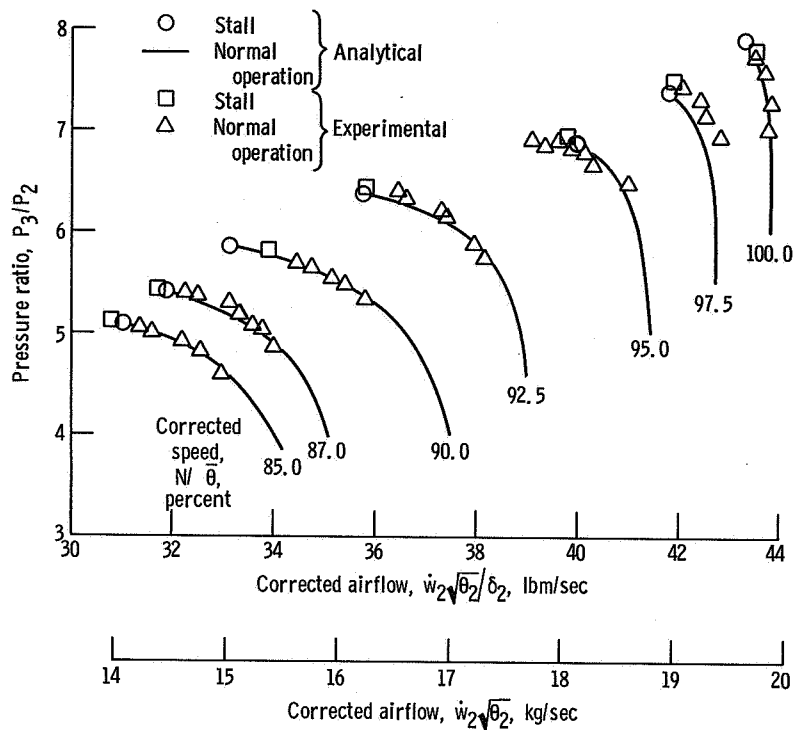


Figure 8. - Compressor map for off schedule inlet guide vanes and interstage bleeds.

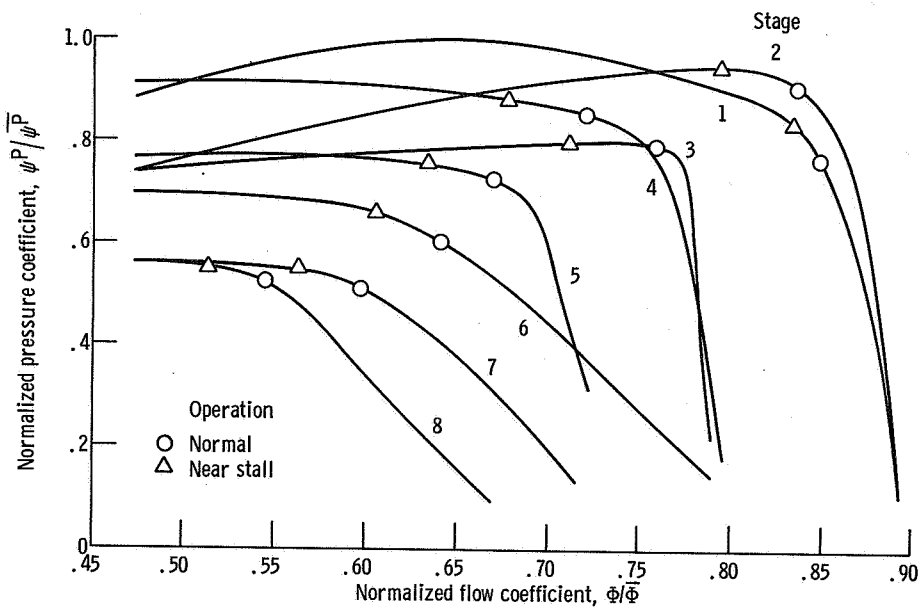


Figure 9. - Stage pressure maps including operating points for design speed.

an operating point just prior to the limit cycle. Figure 9 contains the pressure coefficient curves for each stage and the two operating points at 100 percent corrected speed. Figure 10 contains the same data obtained at 80 percent corrected speed. The compressor variable geometry is fully closed at 100 percent corrected speed and fully open at 80 percent. The effects of the variable geometry are reflected in the different first stage characteristics and in the reduced flow through the later stages at the 80 percent operating condition.

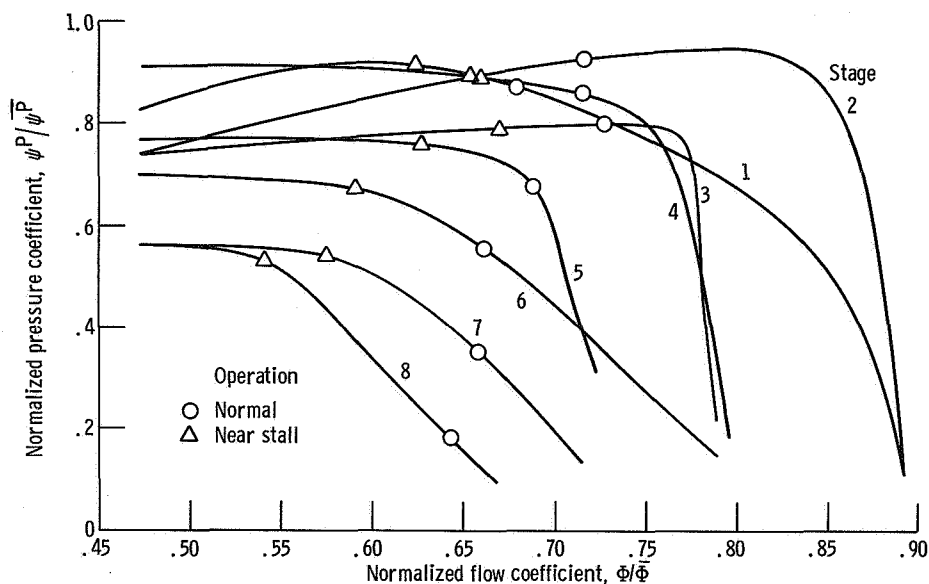


Figure 10. - Stage pressure maps including operating points for 80 percent of design speed.

From the data plotted for the 100 percent corrected speed case in figure 9, it can be seen that the normal operating condition falls on the negative slope portion of the pressure coefficient curves for all of the stages. As the stability boundary is approached, all of the stages move toward operation at a lower negative slope. Second stage operation falls on the horizontal portion of the stage characteristic and the third stage is operating in a region with positive slope. For operation at 80 percent corrected speed shown on figure 10, however, normal operation for the second and third stages is always in the region of positive slope. As the stability boundary is approached, operation of these two stages shifts toward increasing positive slope.

The stage characteristics plotted in these figures are those included in the simulation. It should be noted that they include no sharp discontinuity to represent stage stall. The limit cycle encountered in the simulation, that matches the compressor stall line, is thus assumed to be a system stability phenomenon associated with the system gains and phase lags. Stall prediction by this method cannot be expected to duplicate stall caused by ex-

treme degradation of individual stage performance at a specific operating condition, unless operation under such conditions can be included in the stage characteristics. It should be noted that the simulation is not a valid representation of the compressor once the stability boundary is crossed.

REMARKS AND CONCLUSIONS

A high frequency analytical model for a jet engine compressor has been presented. The modeling technique was applied to the eight-stage axial-flow compressor of the J 85-13 engine. The stability boundary of the compressor simulation agrees closely with the stall line of the actual jet engine compressor.

It was found, that it is necessary to include lumped volume representations for the gas dynamics of each compressor stage to achieve agreement between the simulation stability boundary and the compressor stall line.

Plots of the stage pressure characteristic for each compressor stage were presented for two compressor corrected speeds. The normal stage operating point and an operating point just prior to the stability boundary were indicated on each of the pressure characteristic curves. From these plots it was concluded that the stability boundary is a function of the combined nonlinear system gains and the volume dynamics.

The compressor stability boundary is strongly influenced by the stage characteristics. The overall results are thus dependent on the accuracy of the stage characteristics, and the stall line prediction is dependent on the characteristics at the lower values of the flow parameter. The representation is one dimensional, and, thus, two-dimensional phenomena such as rotating stall and the effects of spatial distortion of the inlet flow field cannot be evaluated. If the technique proves successful in the prediction, the stall characteristics of other compressors, it will provide a useful tool for future compressor design programs.

Lewis Research Center,
National Aeronautics and Space Administration,
Cleveland, Ohio, July 10, 1969,
720-07.

APPENDIX A

SYMBOLS

A	area, ft^2 ; m^2
a	speed of sound, ft/sec; m/sec
C	coefficient, $\text{rpm}^2/^\circ\text{R}^2$; rpm^2/K^2
C_p	specific heat at constant pressure, $\text{Btu}/(\text{lbm})(^\circ\text{R})$; $\text{J}/(\text{kg})(\text{K})$
C_v	specific heat at constant volume, $\text{Btu}/(\text{lbm})(^\circ\text{R})$; $\text{J}/(\text{kg})(\text{K})$
g	gravitational constant, unit force/unit mass
h	enthalpy, Btu/lb_m ; J/kg
J	mechanical equivalent of heat, ft-lbf/Btu; N-m/J
K	coefficient, $(\text{rpm})(\text{sec})/\text{ft}$; $(\text{rpm})(\text{sec})/\text{m}$
k	bleed flow coefficient, $^\circ\text{R}/\text{sec}$; K/sec
L	length, ft; m
M	Mach number
N	rotational speed, rpm
P	pressure, lb/ft^2 ; N/m^2
R	universal gas constant, $\text{ft}/^\circ\text{R}$; m/K
r	radius, in.; m
T	temperature, $^\circ\text{R}$; K
t	time, sec
U	rotor speed, ft/sec; m/sec
u	internal energy, Btu/lb ; J/kg
V	volume, ft^3 ; m^3
v	velocity, ft/sec; m/sec
v_z	axial velocity, ft/sec; m/sec
\dot{W}	weight flow, lb/sec; kg/sec
α	coefficient, $360 (\text{in.})(\text{sec})/(\text{ft})(\text{min})$; $30 (\text{m})(\text{sec})/(\text{m})(\text{min})$
β	rotor air inlet angle, deg

γ	ratio of specific heats
δ	ratio of total pressure to standard atmospheric pressure nondimensional
Θ	ratio of total temperature to standard atmospheric temperature
ρ	weight density, lb/ft ³ ; kg/m ³
Φ	flow coefficient
ψ^P	pressure coefficient
ψ^T	temperature coefficient

Subscripts:

b	variable associated with stage bleed
c	variable associated with the stage characteristic
n	stage number designation
r	reference state
s	static condition
t	total condition
v	variable associated with the stage volume
1, 2, 3, . . . , 8	stage numbers

Superscript:

—	maximum value of quantity used for normalizing
---	--

APPENDIX B

STEADY-STATE COMPRESSOR REPRESENTATION

The analytical modeling of the steady-state compressor characteristics is based on the stage-stacking technique. This technique, which is discussed in reference 1, uses a pair of two-dimensional curves for each stage. The individual stage performance, described by a pressure coefficient ψ^P and a temperature coefficient ψ^T , is assumed to be a function of a flow coefficient Φ . The coefficients are mathematically described by

$$\left. \begin{aligned} \psi^P &= \frac{2gJ \Delta h'_t}{U^2} \\ \psi^T &= \frac{2gJ \Delta h_t}{U^2} \\ \Phi &= \frac{v_z}{U} \end{aligned} \right\} \quad (B1)$$

The ideal total enthalpy rise for the n^{th} stage can be related to the stage total pressure ratio from

$$\Delta h'_{tc, n} = C_p T_{tv, n-1} \left[\left(\frac{P_{tc, n}}{P_{tv, n-1}} \right)^{(\gamma-1)/\gamma} - 1 \right] \quad (B2)$$

The adiabatic enthalpy rise can be determined from

$$\Delta h_{tc, n} = C_p (T_{tc, n} - T_{tv, n-1}) \quad (B3)$$

and the stage wheel speed U from

$$U = \frac{\pi N r}{\alpha} \quad (B4)$$

The stage inlet conditions are associated with the conditions in the preceding volume and the variables are subscripted accordingly. The stage exit conditions are, however, as-

sociated with the stage itself. Assuming that the n^{th} compressor stage is preceded by the $n - 1$ volume, equations (B1) can be combined with (B2) to (B4) to form the following set of equations for the n^{th} stage

$$\psi_n^P = \frac{C_n T_{tv, n-1}}{N^2} \left[\left(\frac{P_{tc, n}}{P_{tv, n-1}} \right)^{2/7} - 1 \right]$$

$$\psi_n^T = \frac{C_n}{N^2} (T_{tc, n} - T_{tv, n-1})$$

$$\Phi_n = \frac{K_n}{N} v_{zc, n} \quad (\text{B5})$$

where

$$C_n = \frac{2gJC_p(\alpha)^2}{\pi^2 r_n^2}$$

$$K_n = \frac{\alpha}{\pi r_n}$$

The flow coefficient Φ is defined as the ratio of the axial flow velocity to a mean rotor velocity. Introducing the square root of the stage corrected temperature into the relation for Φ given in equations (B1), the flow coefficient becomes

$$\Phi = \frac{v_z / \sqrt{\Theta}}{U / \sqrt{\Theta}} \quad (\text{B6})$$

The axial velocity v_z can be computed from the flow, total pressure and total temperature at the stage inlet. The flow and the axial velocity are related by

$$v_z = \frac{\dot{W}}{\rho_s A} \quad (\text{B7})$$

Eliminating the density from (B7) with a state equation of the form

$$P_s = \rho_s RT_s$$

results in

$$v_z = \frac{\dot{W}R}{A} \frac{T_s}{P_s} \quad (\text{B8})$$

or

$$v_z = \frac{\dot{W}R}{A} \frac{T_t}{P_t} \left(1 + \frac{\gamma - 1}{2} M^2\right)^{1/(\gamma-1)} \quad (\text{B9})$$

Equation (B9) can be rewritten in terms of corrected parameters as

$$\frac{v_z}{\sqrt{\Theta}} \rho_{\text{tr}} = \frac{\dot{W}\sqrt{\Theta}}{A\delta} \left(1 + \frac{\gamma - 1}{2} M^2\right)^{1/(\gamma-1)}$$

or

$$\frac{\dot{W}\sqrt{\Theta}}{A\delta} = \frac{v_z}{\sqrt{\Theta}} \left(1 + \frac{\gamma - 1}{2} M^2\right)^{-1/(\gamma-1)} \rho_{\text{tr}} \quad (\text{B10})$$

It can be shown from the energy equation that

$$\frac{v^2}{a_t^2} = \frac{2JC_p}{\gamma R} \left(1 - \frac{T_s}{T_t}\right) \quad (\text{B11})$$

or

$$\frac{T_s}{T_t} = 1 - \frac{\gamma - 1}{2} \frac{v^2}{a_t^2}$$

thus, since

$$\frac{T_s}{T_t} = \left(1 + \frac{\gamma - 1}{2} M^2\right)^{-1} = \left(1 - \frac{\gamma - 1}{2} \frac{v^2}{a_t^2}\right) \quad (\text{B12})$$

Combining equations (B10) and (B12) results in

$$\frac{\dot{W}\sqrt{\Theta}}{A\delta} = \frac{v_z}{\sqrt{\Theta}} \left[1 - \left(\frac{v}{\sqrt{\Theta}} \right)^2 \frac{1}{2gJC_p T_{tr}} \right]^{1/(\gamma-1)} \rho_{tr} \quad (B13)$$

It should be noted that the unsubscripted velocity variable v introduced in equation (B11) is the magnitude of the velocity vector and not the axial velocity component v_z . If the air flow approaches the rotor inlet at an angle β

$$v_z = v \cos \beta \quad (B14)$$

and equation (B13) becomes

$$\frac{\dot{W}\sqrt{\Theta}}{A\delta} = \frac{v_z}{\sqrt{\Theta}} \left[1 - \left(\frac{v_z}{\sqrt{\Theta}} \right)^2 \frac{1}{2gJC_p T_{tr} \cos^2 \beta} \right]^{1/(\gamma-1)} \rho_{tr} \quad (B15)$$

For the n^{th} stage the flow parameter Φ_n can be described by

$$\Phi_n = \frac{K_n}{N} \frac{v_{zc, n}}{\sqrt{\Theta_{v, n-1}}} \quad (B16)$$

and the corrected axial velocity $v_{zc, n}/\sqrt{\Theta_{v, n-1}}$ is determined from solutions of equation (B15) rewritten for n^{th} stage as

$$\frac{\dot{W}_{c, n}\sqrt{\Theta_{v, n-1}}}{A_n \delta_{v, n-1}} = \frac{v_{zc, n}}{\sqrt{\Theta_{v, n-1}}} \left[1 - \left(\frac{v_{zc, n}}{\sqrt{\Theta_{v, n-1}}} \right)^2 \frac{1}{2gJC_p T_{tr} \cos^2 \beta_n} \right]^{1/(\gamma-1)} \rho_{tr} \quad (B17)$$

APPENDIX C

STAGE GAS DYNAMICS

The gas dynamics of each compressor stage is assumed to occur in an equivalent stage volume. The stage volume is conceptually located just downstream of the stage pressure and temperature rise characteristics. The stage gas dynamics are represented by continuity, energy, and momentum balances across the volume.

Assuming no work is performed in the volume and that the net heat input is negligible, an energy balance can be written for the n^{th} volume as

$$V_n \frac{d}{dt} (\rho_{sv, n} u_{tv, n}) = h_{tc, n} \dot{W}_{c, n} - h_{tv, n} \dot{W}_{c, n+1} \quad (C1)$$

Noting that $u_t = C_v T_t$ and that $h_t = C_p T_t$, equation (C1) becomes

$$\frac{d}{dt} (\rho_{sv, n} T_{tv, n}) = \frac{\gamma}{V_n} (T_{tc, n} \dot{W}_{c, n} - T_{tv, n} \dot{W}_{c, n+1}) \quad (C2)$$

To determine the density of the gas in the stage volume, it is assumed that the rate of change of the static density is proportional to the net weight flow:

$$\frac{d}{dt} (\rho_{sv, n}) = \frac{1}{V_n} (\dot{W}_{c, n} - \dot{W}_{c, n+1}) \quad (C3)$$

The total pressure in the stage volume is calculated from an equation of state of the form

$$P_{tv, n} = R \left(1 + 0.2 M_{v, n}^2 \right)^{5/2} (\rho_{sv, n} T_{tv, n}) \quad (C4)$$

A momentum balance written across the stage and its associated volumes is used to provide an expression for the determination of weight flow. It is assumed that flow acceleration is caused by the difference between the static compressor head rise $\Delta P_{sc, n}$ and the head rise $(P_{sv, n} - P_{sv, n-1})$ imposed by the adjacent volumes. Neglecting convective momentum terms, the above assumption yields

$$\frac{d}{dt} (\dot{W}_{c, n}) = \frac{A_n g}{L_n} \left[\Delta P_{sc, n} - (P_{sv, n} - P_{sv, n-1}) \right] \quad (C5)$$

The stage inlet conditions, however, are the conditions in the inlet volume and, thus, $\Delta P_{sc, n} = P_{sc, n} - P_{sv, n-1}$ and equation (C5) becomes

$$\frac{d}{dt} (\dot{W}_{c, n}) = \frac{A_{ng}}{L_n} (P_{sc, n} - P_{sv, n}) \quad (C6)$$

Assuming the Mach number at the stage exit and in the volume are the same, equation (C6) can be written as

$$\frac{d}{dt} (\dot{W}_{c, n}) = \frac{A_{ng}}{L_n} \left(1 + 0.2 M_{v, n}^2\right)^{-7/2} (P_{tc, n} - P_{tv, n}) \quad (C7)$$

Equations (C2) to (C4) and (C7) provide a representation for the gas dynamics of the n^{th} stage volume. In the computer simulation of these equations, the distinction between static and total pressures was dropped. This simplification resulted in neglecting the Mach number corrections in equations (C4) and (C7). The interstage Mach numbers encountered in the compressor are less than 0.5. The range of the corrections in equations (C4) and (C7) are thus,

$$1.0 < \left(1 + 0.2 M^2\right)^{5/2} < 1.13$$

$$0.84 < \left(1 + 0.2 M^2\right)^{-7/2} < 1.0$$

The error introduced by this simplification is, thus, approximately equivalent to a 15 percent change in the equation coefficients in the worst case. With the computer formulation used, the approximation is reflected in dynamic coefficients and does not alter the steady-state results.

Figure 11 contains a block diagram of the computational scheme used for the dynamics of a typical stage. The coefficients used in the simulation are represented by numbered circles and the neglected corrections by lettered dashed circles. Noting that the integrator inputs are nulled in the steady state, it can be shown that neglecting the Mach number corrections results in

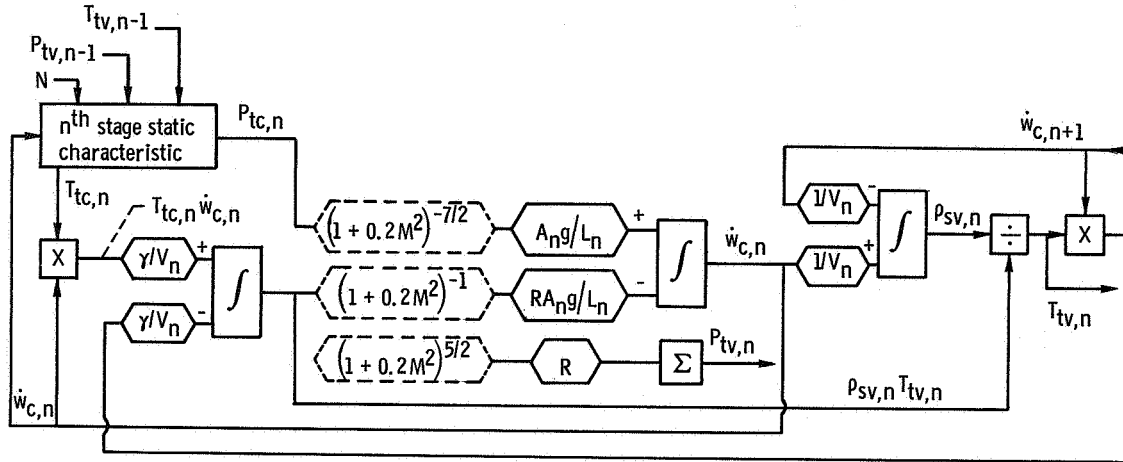


Figure 11. - Block diagram for n^{th} stage computational scheme.

$$\left. \begin{aligned}
 \frac{1}{V_n} (\dot{W}_{c,n} - \dot{W}_{c,n+1}) &= 0 \\
 \frac{\gamma}{V_n} (T_{tc,n} \dot{W}_{c,n} - T_{tv,n} \dot{W}_{c,n+1}) &= 0 \\
 \frac{A_n g}{L_n} P_{tc,n} - \frac{A_n g}{L_n} P_{tv,n} &= 0
 \end{aligned} \right\} \quad (C8)$$

in the steady state. Equations (C8) thus yield,

$$\left. \begin{aligned}
 \dot{W}_{c,n} &= \dot{W}_{c,n+1} \\
 T_{tc,n} &= T_{tv,n} \\
 P_{tc,n} &= P_{tv,n}
 \end{aligned} \right\} \quad (C9)$$

in the steady state. Thus, the steady-state results are unaffected by the approximations in the volume dynamics.

REFERENCES

1. Johnsen, Irving A.; and Bullock, Robert O., eds.: Aerodynamic Design of Axial-Flow Compressors. NASA SP-36, 1965.
2. Drabek, S.: Stall Control. Paper presented at the Joint Conference of the ASME Gas Turbine Power and Hydraulic Divisions, Houston, Texas, Mar. 1960.
3. Gabriel, D.; Wallner, L.; Lubick, R.; and Vasu, G.: Some Effects of Inlet Pressure and Temperature Transients on Turbojet Engines. Aeron. Eng. Rev., vol. 16, no. 9, Sept 1957, pp. 54-59.
4. Kuhlberg, J. F.; Sheppard, D. E.; King, E. O.; and Baker, J. R.: Compressor Response to Inlet Pressure Fluctuations - The Dynamic Simulation of Turbine Engine Compressors. Paper 69-486, June 1969.
5. Calogeras, James E.: Experimental Investigation of Dynamic Distortion in a Mach 2.50 Inlet with 60 Percent Internal Contraction and Its Effect on Turbojet Stall Margin. NASA TM X-1842, 1969.